16A.6

FINE-SCALE OBSERVATIONS OF A DRYLINE DURING THE INTERNATIONAL H_2O PROJECT

Christopher C. Weiss
Texas Tech University, Lubbock, Texas

Howard B. Bluestein
University of Oklahoma, Norman, Oklahoma

Andrew Pazmany
ProSensing, Inc., Amherst, Massachusetts

1. INTRODUCTION

The dryline in the southern Plains of the United States can be thought of as the intersection of the top of a surface-based layer of virtually cool, moist air originating over the Gulf of Mexico and the sloping terrain east of the Rocky Mountains. The axis of the dryline represents a three-dimensional region of enhanced low-level convergence. Therefore, it also denotes a zone in which there is upward vertical motion. Owing to the strong vertical wind shear that is often characteristic of the dryline environment, storms that form on the dryline often attain supercellular attributes, thereby carrying the attendant threat of large hail, damaging winds and tornadoes.

During the spring of 2002, a multi-agency field experiment, the International H_2O Project (IHOP), was conducted over the central and southern Plains. The primary goal of this project was the "improved characterization of the four-dimensional distribution of water vapor and its application to improving the understanding and prediction of convection" (UCAR/ATD 2002). The convection initiation (CI) component of this project was focused on resolving the kinematics of surface boundaries, particularly heterogeneities that would yield clues to the preferential development of convection (e.g., triple points). Multiple ground-based and aircraft-based measurement platforms were employed for this purpose.

As part of this cooperative effort, the W-band (3 mm wavelength) radar from the University of Massachusetts (UMass) (Bluestein and Pazmany 2000) gathered data on several IHOP case days. Since the quality of the data on 22 May 2002 was superior to that obtained on the rest of the operations days, this date has been chosen as a focus for this study. Owing to the very fine beamwidth of the radar (0.18 degrees), previously unresolved dryline spatial structure was observed.

The primary scientific objective of this research is to resolve previously unseen finescale motions of the dryline. Knowing these motions helps us better visualize the contribution of each individual air mass at the dryline interface, and will ultimately lead to better conceptual models of modes of success and failure of CI in the dryline convergence zone (DCZ).

2. W-BAND RADAR CHARACTERISTICS

The primary data sets used for this study were collected with the W-band radar. The principal scatterering source for the power returned to the W-band radar was most likely insects (Wilson and Schreiber 1986). Since the wavelength was comparable to the size of the targets, Mie scattering was the dominant source of returned power. The minimum detectable signal for the W-band radar was –35 dBZ_e at a range of 1 km from the radar. The average reflectivity in convergence zones at this range (shown later) was about –20 dBZ_e, representing a returned power over 30 times the minimum detectable signal.

A number of scanning strategies were utilized during IHOP, three of which were as follows:

1) Vertical antenna – antenna pointed at 86 degrees (maximum elevation allowed by the positioner) and driven across the boundary. The result was a time series of vertical velocity data, which was converted to a spatial profile using recorded GPS data.

2) Stationary RHI (SRHI) – stationary data collection in which the antenna was rotated from ~0-86 degrees in elevation. Multiple vertical

sectors of radial velocity data were obtained in this manner. Although useful for tracking reflectivity and diagnosing radial velocity, the *u* and *w* components could not be retrieved independently with such a collection strategy.

3) Rolling RHI (RRHI) – 0-86 degree RHIs collected with the platform in motion. The radial velocity was adjusted for platform motion. The principles of pseudo-dual Doppler analysis could be applied to data taken in such a manner to retrieve the individual *u* and *w* wind components.

3. RESULTS FROM VERTICAL ANTENNA DEPLOYMENT (2221-2235 UTC)

From 2221-2235 UTC, the UMass W-band executed a westward-moving vertical antenna deployment across the double dryline along US Highway 270 near Elmwood, OK in the Oklahoma panhandle. The objective of this deployment was to obtain a time series of vertical velocity in the near-dryline environment. The vehicle maintained a nearly constant speed of 27 m s^{-1} during the traverse.

The Shared Mobile Atmospheric Research and Training Radar (SMART-R) (FIG. 1a) (Biggerstaff and Guynes 2000) and NCAR S-band Polarimetric Radar (SPOL) (FIG. 1b) (http://www.atd.ucar.edu/rsf/spol/spol.html) both indicated a fineline associated with the eastern DCZ. This boundary was oriented north-northeast to south-southwest. Therefore, the traverses were not precisely normal, but rather formed a small angle from normal, to the boundary. A secondary fineline was evident to the west of the "primary" (i.e., targeted) dryline. Though not recognized at the time of data collection, the UMass W-band radar transected this secondary feature just before the termination of the data collection leg (FIGS. 1a, 1b). Both finelines were collocated with a specific humidity change of 2-2.5 g kg^{-1} over a distance of approximately 1 km (FIG. 1c).

The time section of reflectivity from this leg (FIG. 2) shows clearly the eastern DCZ as an area of reflectivity in excess of –15 dBZ_e. The reflectivity maxima was associated with a local concentration of boundary-layer scatterers, primarily insects (Wilson and Schreiber 1986). To a first approximation, these insects are treated as passive and are therefore representative of the wind that is transporting them. Convergence regions, like the one in FIG. 2, therefore represent areas with a higher density of insects (assuming the insect size distribution was the same everywhere). The plume of highest reflectivity was nearly vertical, consistent with previous observations of a nearly vertical dryline interface (e.g., Crawford and Bluestein 1997). A mobile mesonet (Straka et al. 1996) traverse of the eastern dryline revealed a 6 ^{o}C increase in dewpoint over approximately 1 km as the probe headed eastward (FIG. 3). Coincident with the dewpoint rise was a sharp pressure increase of 4 hPa. A portion of this pressure rise was due to an elevation drop (calculated from the hypsometric equation to be 2.6 hPa), but there was a residual pressure increase that was in part due to the virtual temperature decrease. Assuming that the horizontal changes in temperature and dewpoint measured at the surface were also constant through the lowest 1 km AGL, the hydrostatic pressure increase was 0.2 hPa. Thus, a residual pressure increase of 1.2 hPa remained, possibly due to non-hydrostatic effects.

Approximately 9 km to the west of the primary (eastern) dryline was the secondary (western) dryline. The feature, though quite subtle in PPI reflectivity imagery from SMART-R 1 (FIG. 1a) and SPOL (FIG. 1b), was very distinct in the UMass W-band cross section (FIG. 2). Both the eastern and western convergence zones were nearly vertical in the lowest 1-1.5 km AGL, above which a considerable tilt to the east with height was evident. DCZs with a large downshear tilt with height have been identified as being less favorable for the development of deep convection as ascending parcels have a greater chance of advecting out of the DCZ before reaching the LCL and LFC (Ziegler and Rasmussen 1998).

Minima in reflectivity were observed in the dryline interface at approximately 1.5 km AGL. One of these areas ("D_1" in FIG. 2) was immediately to the east of the surface position of the eastern DCZ. The other position ("D_2" in FIG. 2) was about 4 km to the east of the DCZ. The vertical velocity data from the same leg (FIG. 4) showed a correlation between these low reflectivity intrusions and subsiding air motion [considering the fringe vertical velocity values on the border of these reflectivity-void regions and others to the west of the eastern DCZ]. Since the source for the scatterers (i.e., insects) is the surface, the scatterer concentration is nearly zero at higher altitudes (e.g., above the boundary layer). Therefore, downward motion represents transport from a region where there is a dearth of insects, and is therefore associated with a lack of radar reflectivity (D. Leon, University of Wyoming, 2004, personal communication).

4. RESULTS FROM ROLLING RHI DEPLOYMENT (0007-0036 UTC)

From 0007-0036 UTC, the UMass W-band executed a westward-moving rolling RHI deployment across the eastern dryline. The geometry of the scanning strategy permitted the overlap of rays. Therefore, individual points in space received many “looks” from the radar, separated in both time and look angle. Assuming stationarity for the time period between the looks (a maximum of 60 s in this case), pseudo-multiple Doppler principles (Hildebrand et al. 1996) were employed to synthesize the *u* and *w* wind components in the plane approximately normal to the dryline.

A variational analysis was applied to rolling RHI data taken on the (eastern) 22 May 2002 dryline as it retrograded back towards the west in the early evening hours (0007-0036 UTC (23 May 2002)). The retrogression was not uniform as there was evidence of wave activity along the dryline interface. Data from various radar platforms permitted an estimated retrogression speed between 2 and 5 m s^{-1} during the period of the traverse. The UMass radar platform traveled at a nearly constant velocity of 13 m s^{-1} towards the west as RHI sweeps were taken from the rear horizon up through ~86 degrees above the rear horizon. The raw time series of data were post-processed to account for truck velocity and pitch before the analysis was performed.

A composite reflectivity image for the traverse (FIG. 5) showed the pronounced eastward tilt of the dryline interface with height during retrogression. As seen in the vertical antenna deployment, the DCZ appeared as a maximum in reflectivity, presumably due to the local increase in insect concentration in this region. The domain chosen for analysis was the lowest 1 km AGL, where there were no data voids.

The *u*-component of the optimal analysis (FIG. 6a) reveals the upper and lower branches of the dryline secondary circulation quite clearly. The near-surface inflow to the DCZ from the east approached u=-6 m s^{-1} in some areas of the CBL. Above the CBL, strong westerly component winds (i.e., the return flow) were seen, a combination of air parcels from the moist CBL that had ascended in the DCZ (Hane et al. 1997) and parcels from the dry side that had advected up and over the moist CBL. Westerly winds upward of u=15-20 m s^{-1} were seen in the upper portion of the domain (just above 1 km AGL). The altitude of the boundary between easterly and westerly component winds varied between 500 m AGL and over 1 km AGL over the domain; the lowest altitude at which the boundary was seen was ~3 km east and ~12 km east of the dryline. Both of these areas were also coincident with subsiding air.

The DCZ showed up clearly in the *w*-component field (FIG. 6b) as a maximum *w* of 8-10 m s^{-1} (over a very narrow region of ~100 m). The eastward tilt of the DCZ with height was again present. A small area of descent was evident at ~500 m AGL approximately 3 km to the east of the surface position of the DCZ (leftmost arrow in FIG. 6b). The position of this descending motion was similar to that shown for the vertical antenna deployment earlier and the airborne Doppler case study of Weiss and Bluestein (2002), but lacked the vertical continuity present in the latter case. More vertically continuous areas of subsidence were apparent farther to the east of the DCZ, at and around approximately 6, 8 and 13 km to the east of the dryline (indicated by rightmost three arrows in FIG. 6b).

Zooming in on the DCZ, one can still see very clearly the discontinuity in the *u*-component (FIG. 7a) and *w*-component fields at the dryline interface (FIG. 7b) and the rotor circulation on the head of the DSC. From FIGS. 7a and 7b it is clear that the easterly component winds at the surface extended west of the area of maximum upward motion.

5. SUMMARY

On the afternoon of 22 May 2002 during IHOP, a unique data set was collected for a double-dryline event in the Oklahoma panhandle. This data set was comprised of reflectivity and radial velocity measurements from the UMass W-band radar. The narrow beamwidth of the radar afforded very-fine azimuthal resolution of winds at and near the dryline boundaries.

Using two different scanning strategies, the radar was driven westward across both drylines. The DCZ of both drylines was well resolved; a maximum upward vertical velocity of *w* ~ 8 m s^{-1} was measured in a narrow channel approximately 50-100 m wide in the eastern dryline. This magnitude was larger than that reported in earlier mobile Doppler dryline studies. Areas of subsidence were noted away from the DCZ. One such area was found in both UMass W-band and UWKA data approximately 4-5 km east of the DCZ for both drylines.

6. ACKNOWLEDGMENTS

This work was supported by National Science Foundation (NSF) grants ATM-9912097 and ATM-0241037. Dave Leon and Bart Geerts at the University of Wyoming were instrumental in the UWKA intercomparison efforts. Curtis Alexander, Nettie Arnott, Mike Buban, Yvette Richardson and Josh Wurman all assisted in providing mobile radar locations and orientations for the 22 May 2002 case. Ming Xue assisted in the use of ZXPLOT. Brendan Fennell drove the UMass vehicle for the 22 May 2002 data collection.

7. REFERENCES

Biggerstaff, M. I., and J. Guynes, 2000: A new tool for atmospheric research. Preprints, *20th Conf. on Severe Local Storms*, Orlando, FL, Amer. Meteor. Soc., 277-280.

Bluestein H. B., and A. L. Pazmany, 2000: Observations of tornadoes and other convective phenomena with a mobile, 3–mm wavelength, Doppler radar: The spring 1999 field experiment. *Bull. Amer. Meteor. Soc.*, **81**, 2939–2952.

Crawford, T. M., and H. B. Bluestein, 1997: Characteristics of dryline passage. *Mon. Wea. Rev.*, **125**, 463-477.

Hane, C. E., H. B. Bluestein, T. M. Crawford, M. E. Baldwin, and R. M. Rabin, 1997: Severe thunderstorm development in relation to along-dryline variability: A case study. *Mon. Wea. Rev.*, **125**, 231-251.

Hildebrand, P. H., and Coauthors, 1996: The ELDORA/ASTRAIA airborne Doppler weather radar: High resolution observations from TOGA COARE. *Bull. Amer. Meteor. Soc.*, **77**, 213-232.

Straka, J. M., E. N. Rasmussen, and S. E. Fredrickson, 1996: A mobile mesonet for finescale meteorological observations. *J. Atmos. Oceanic Technol.*, **13**, 921-936.

Weiss, C. C., and H. B. Bluestein, 2002: Airborne pseudo-dual Doppler analysis of a dryline-outflow boundary intersection. *Mon. Wea. Rev.*, **130**, 1207-1226.

Wilson, J. W., and W. E. Schreiber, 1986: Initiation of convective storms by radar-observed boundary layer convergence lines. *Mon. Wea. Rev.*, **114**, 2516-2536.

UCAR/ATD, 2002: International H_2O Project (IHOP_2002): Operations Plan, 160 pp.

Ziegler, C. L., and E. N. Rasmussen, 1998: The initiation of moist convection at the dryline: Forecasting issues from a case study perspective. *Wea. Forecasting*, **13**, 1106-1131.

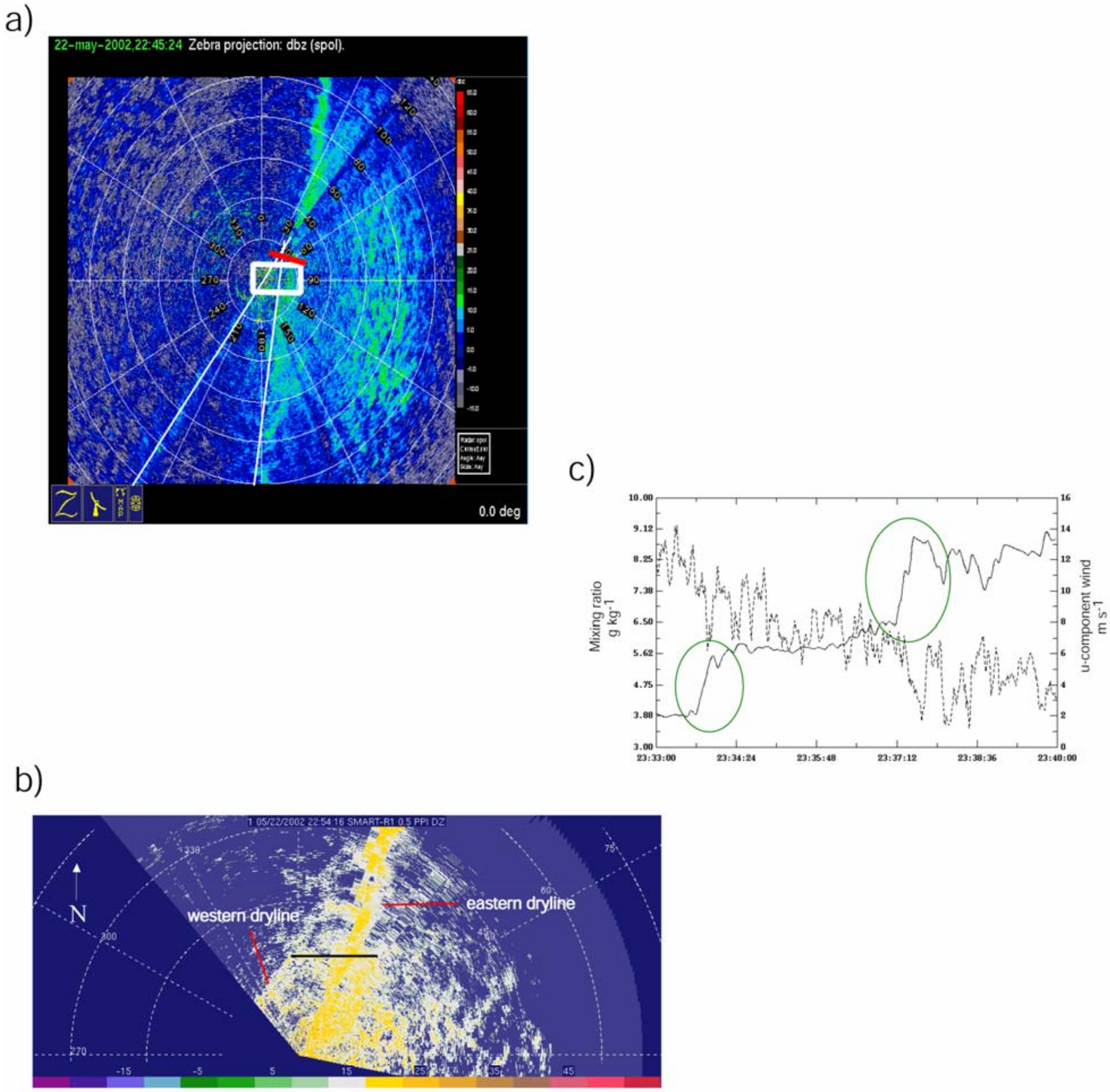

FIG. 1. Reflectivity from a) SPOL and b) SMART-R, and c) Traces of in-situ specific humidity (g kg^{-1}, solid trace) and u-component wind (m s^{-1}, dashed trace) taken aboard the UWKA for the flight leg indicated in a). Reflectivity scale (dBZ) indicated in a) and b). The straight white lines in a) indicate the axes of two separate drylines. The white box in a) represents the domain of operations for the UMass W-band radar. The red line in a) denotes the flight track of the University of Wyoming King Air (UWKA) from 2233-2240 UTC. The black line in b) is the path of the UMass W-band radar, from right to left (east to west). Time (UTC) is indicated along the bottom axis in c). Scales for specific humidity and u-component wind are indicated on the left and right axes, respectively. The two regions of sharp moisture gradient are circled in green.

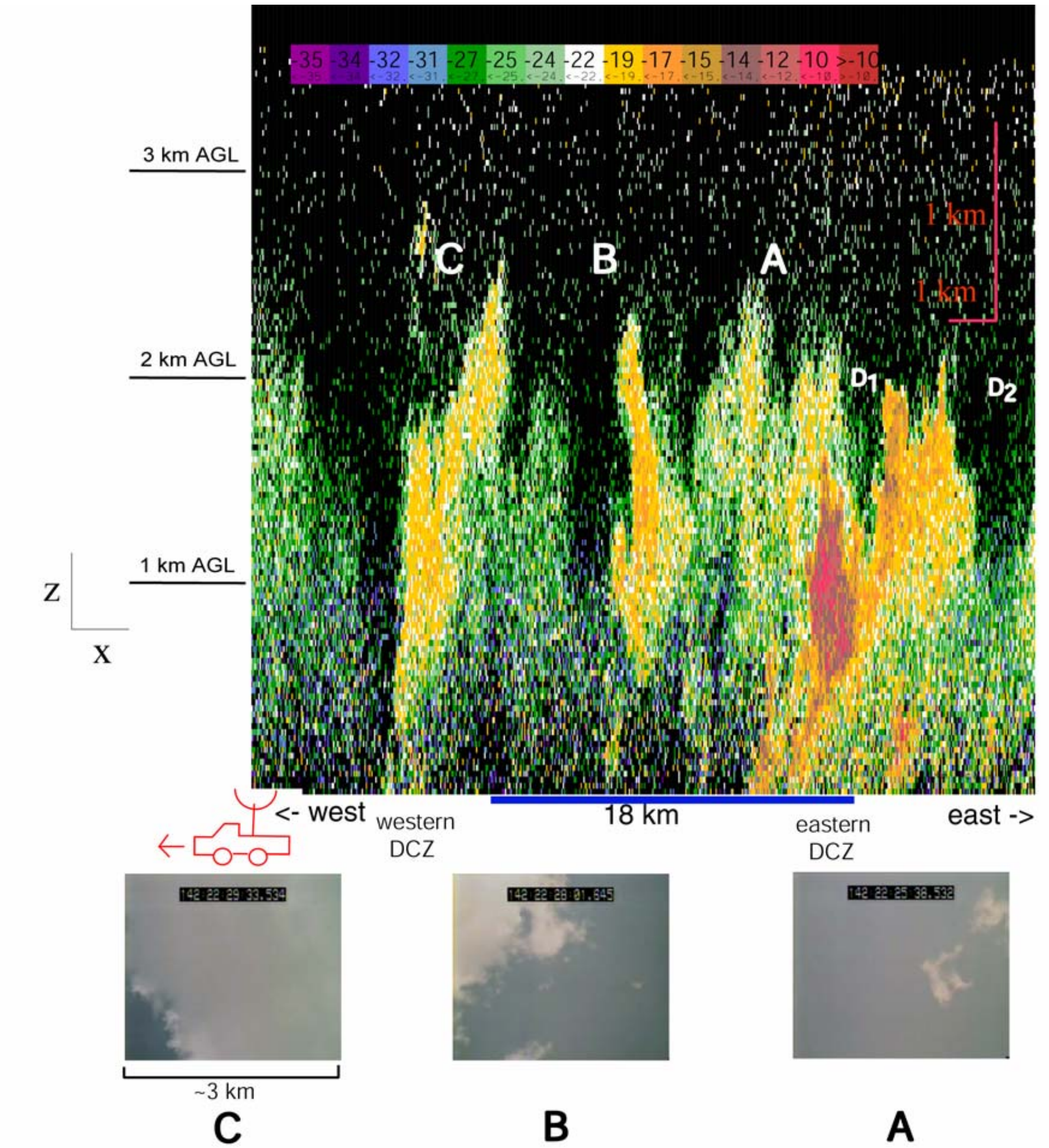

FIG. 2. East-west cross section of reflectivity from the vertical antenna deployment. Reflectivity scale (dBZ_e) is shown at the top. 1 km scales for the horizontal and vertical direction are shown in the upper-right hand corner. Domain size is approximately 18 km wide (east-west) by 3.4 km high. Letters "A", "B" and "C" are the locations of cloud cover discussed in the text. The UMass vehicle was in motion towards the west (left). Labels "D_1" and "D_2" are referred to in the text. Images of video from the W-band boresighted video camera are shown. The blue bar at the base of the reflectivity image is the approximate track of the mobile mesonet probe in FIG. 3.

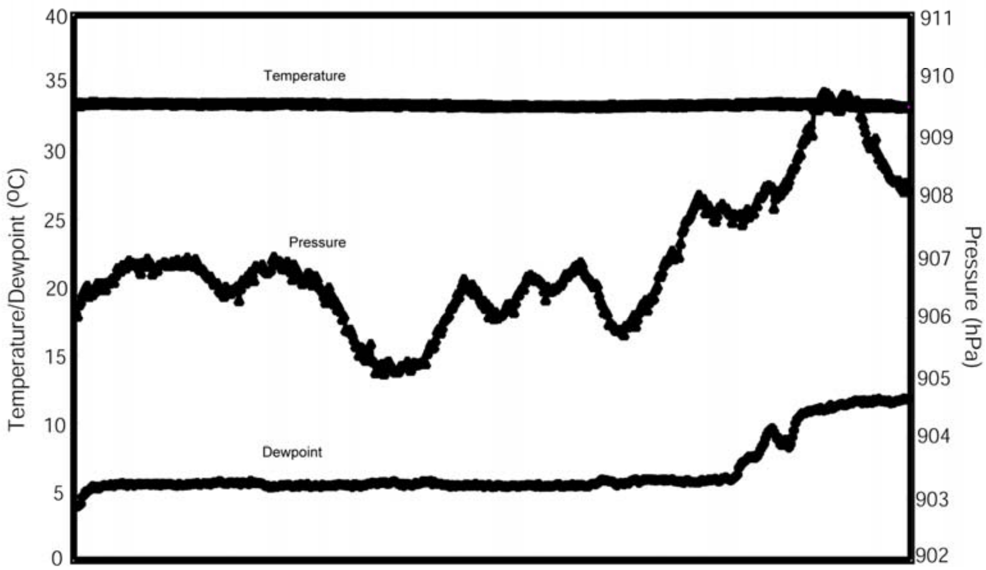

FIG. 3. Temperature, dewpoint (OC, scale on left) and pressure (hPa, scale on right) measured by a mobile mesonet probe from 2237-2245 UTC. Approximate track denoted by blue line in FIG. 2.

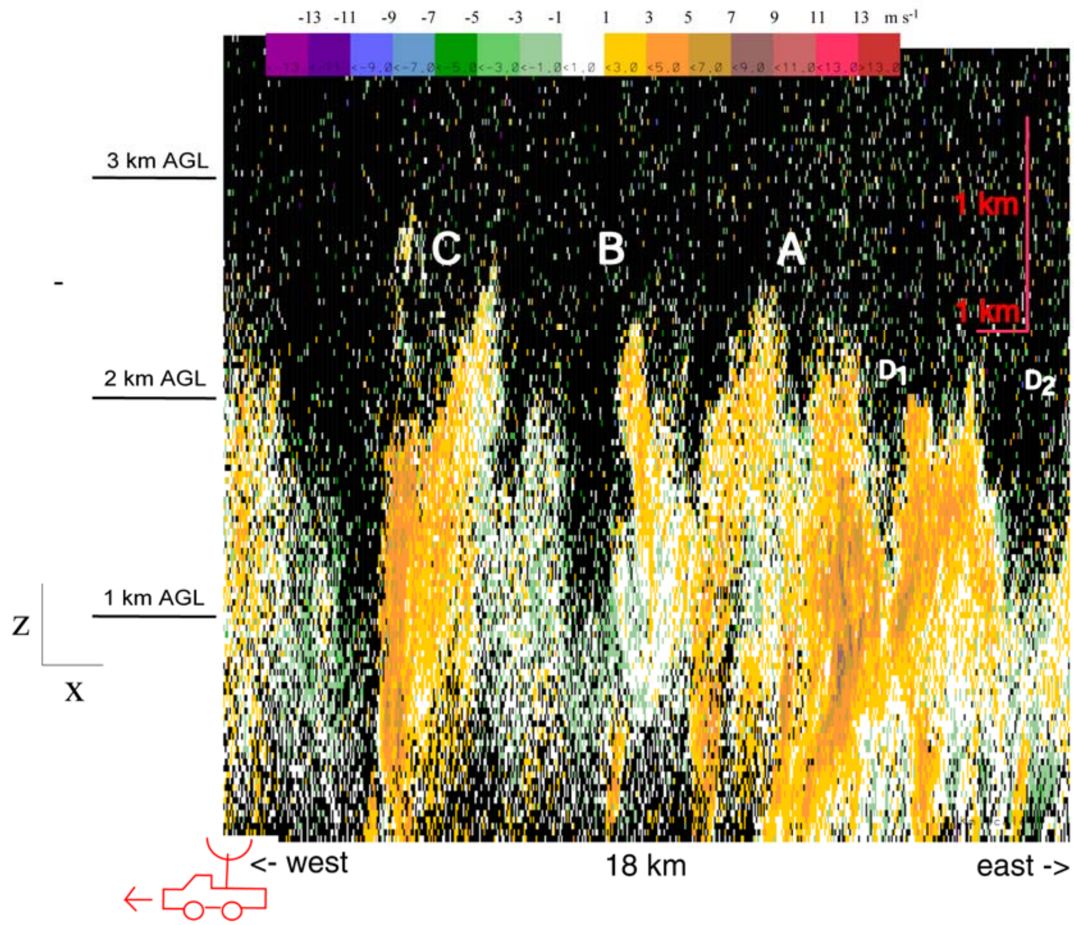

FIG. 4. As in FIG. 2, except colors denote vertical velocity (m s^{-1}). Orange colors indicate upward motion, green colors indicate downward motion. Velocity scale is indicated at the top. Labels "D_1" and "D_2" are referred to in the text.

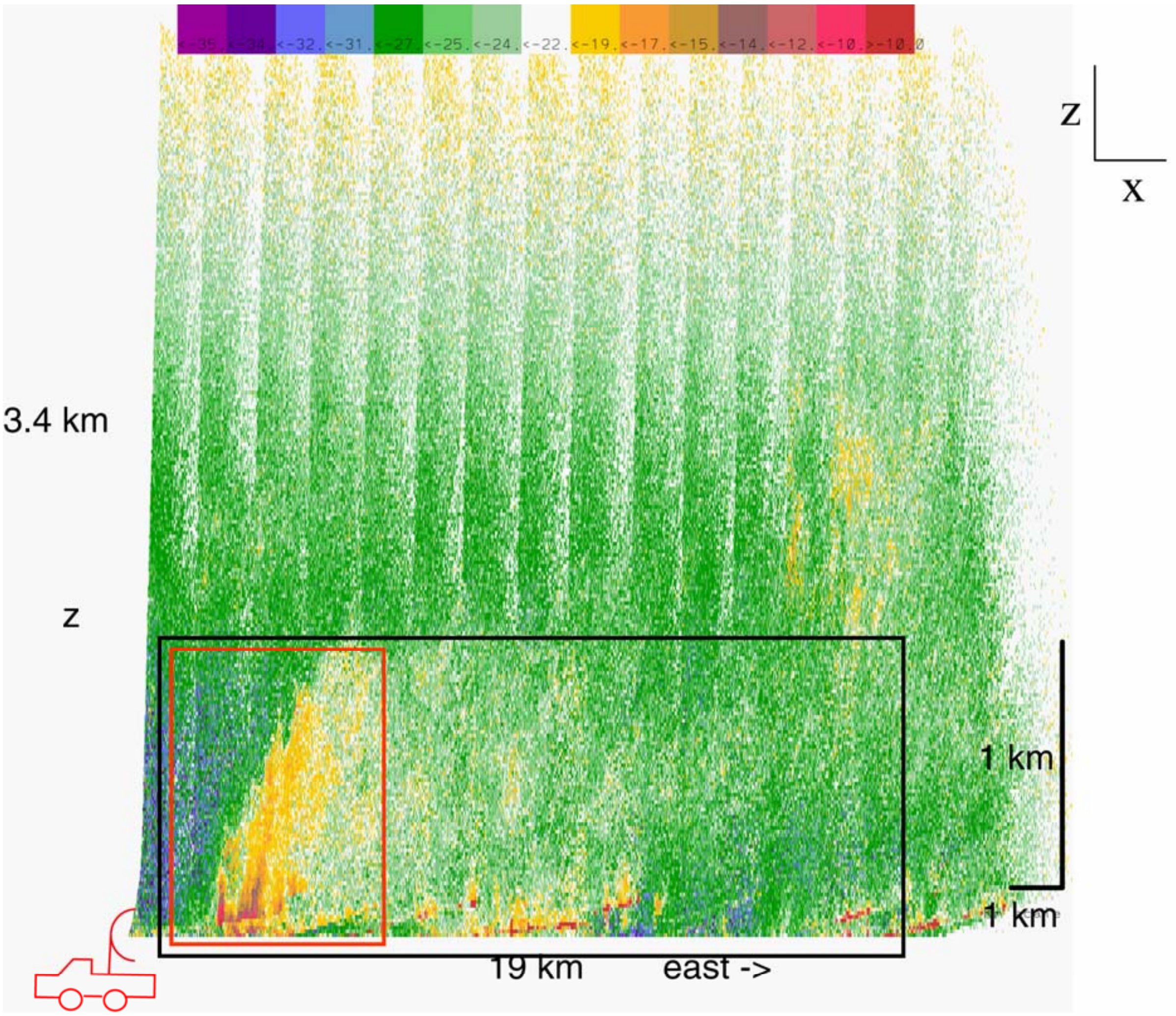

FIG. 5. An east-west display of composite reflectivity from the UMass rolling RHI (2007-2036 UTC). Horizontal and vertical distance scales are indicated in the lower right hand corner. The domain is approximately 19 km wide (east-west) by 3.4 km tall. The black box denotes the domain for the analysis in Fig. 6. The red box denotes the domain for the analysis in Fig. 7.

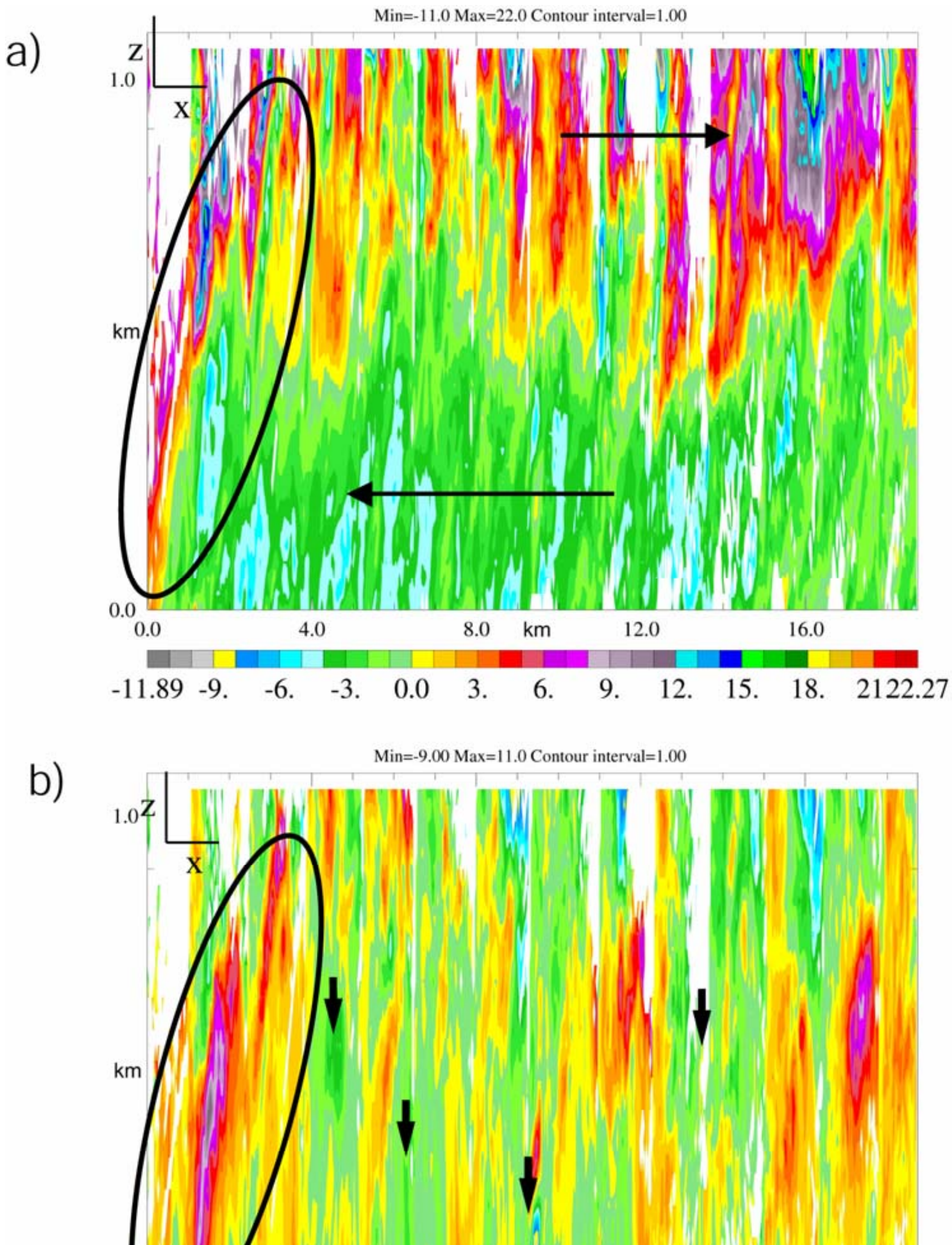

FIG. 6. a) *U*-component wind (m s^{-1}, contoured) and b) *w*-component wind (m s^{-1}, contoured) from the variational analysis of the rolling RHI. Cool colors indicate negative component, warm colors indicate positive component. The oval encircles the DCZ. The arrows in a) denote the easterly inflow to the DCZ at low levels and westerly return flow aloft. The arrows in b) point to areas of descent mentioned in the text. Horizontal and vertical distance scales are indicated. Note that the color scale folds at +12 m s^{-1}.

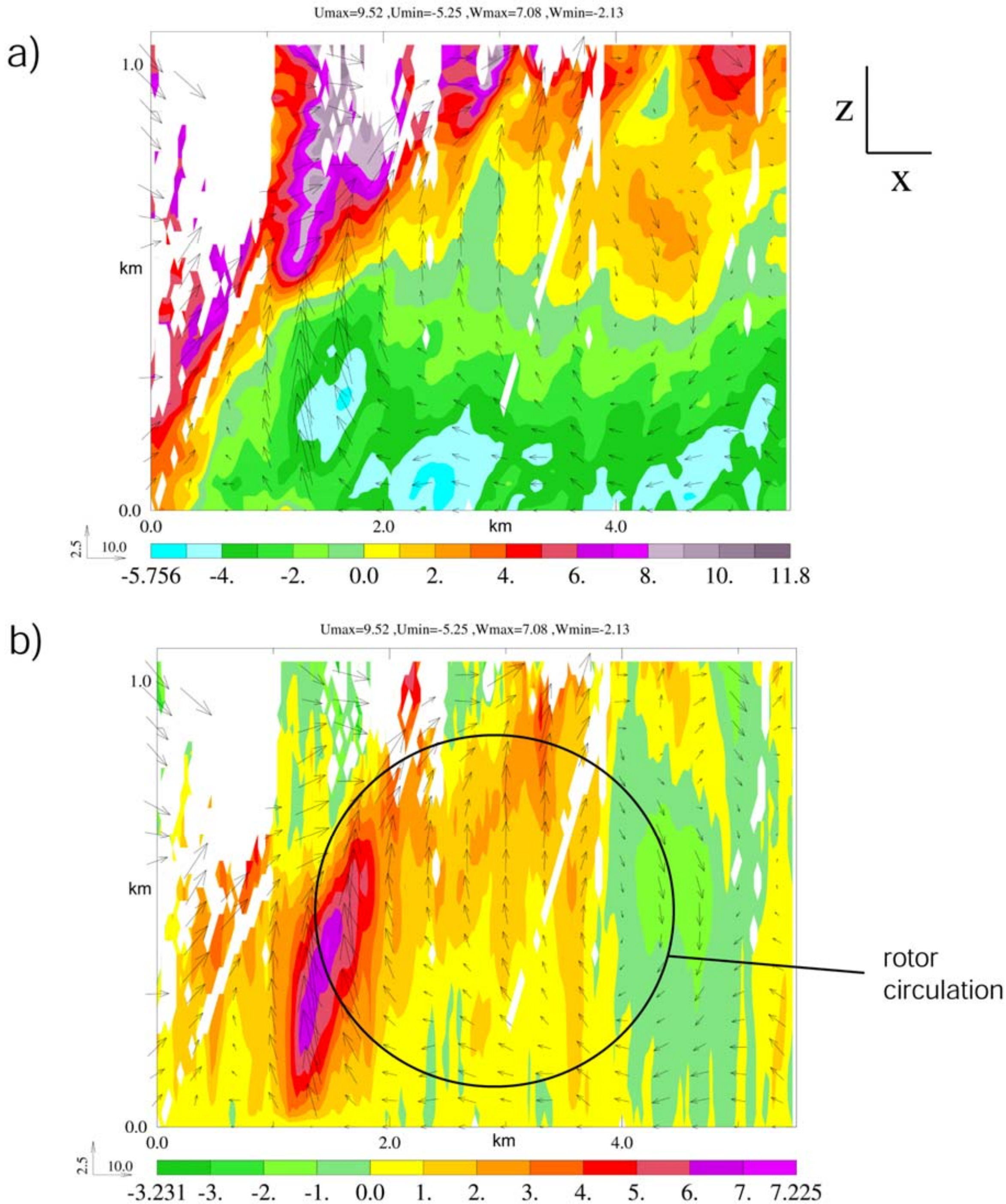

FIG. 7. Analysis a) *u*-component (m s^{-1}, contoured) and b) *w*-component (m s^{-1}, contoured) wind near the retreating dryline interface for the UMass rolling RHI (domain indicated in FIG. 5). Vectors represent *u* and *w* wind components. Horizontal and vertical distance scales are indicated. Data-void areas represent points with fewer than 10 "looks" with the UMass radar. The location of the rotor circulation on the head of the DSC is indicated.